Connectome-Based Reservoir Computing With Coupled Stuart–Landau Oscillators

Tenshin Okuma
Graduate School of Advanced Science and Engineering
Hiroshima University
Hiroshima, Japan

Makoto Fukushima
Graduate School of Advanced Science and Engineering
Hiroshima University
Hiroshima, Japan
mfukushima@hiroshima-u.ac.jp

***Abstract*—Recent computational neuroscience studies have explored the functional roles of the structural connectome in the human brain using the methodology of reservoir computing. However, existing connectome-based reservoir computing models exhibit a spatial scale mismatch between the reservoir edges, derived from the macroscopic connectome, and the reservoir node dynamics, which are inspired by microscopic neural circuitry. To address this issue, here we develop a new connectome-based reservoir computing model. In this model, the spatial scale mismatch is resolved by modeling node dynamics with coupled Stuart–Landau oscillators, which can simulate macroscopic, metastable brain activity. To examine the model's basic properties, we applied it to a standard nonlinear transformation task using sinusoidal and square waves as the input and desired output, respectively. The results demonstrate that regression performance improves with increasing input magnitude and is maximized when the input frequency is close to the frequency peak of the oscillator ensemble with no input. Metastability, which is a key factor in simulating realistic brain dynamics, does not contribute directly to performance during the task; however, an intermediate level of global coupling for the oscillators that yields metastability in the absence of input improves performance robustness against changes in input frequency. This study clarifies the basic characteristics of the new model and reveals the intriguing effects of metastability on reservoir computing performance.**

***Index Terms*—Brain connectivity, Computational neuroscience, Connectome, Coupled oscillators, Reservoir computing.**

I. Introduction

Neuroimaging techniques enable us to map the entire set of macroscopic white matter structural connectivity throughout the human brain, collectively referred to as the human connectome [1]. Recently, the functional properties of the network structure of the connectome have been investigated using the methodology of reservoir computing [2]–[8]. Using a standard reservoir computing model, known as the echo state network [9], these studies regard brain regions in the connectome as nodes in the reservoir layer and replace random connections between nodes with structural connections between brain regions. The functions supported by the network structure of the connectome have been explored by evaluating the performance of connectome-based reservoir computing models in time series processing tasks commonly used in reservoir computing research.

This work was supported by the Japan Society for the Promotion of Science (JSPS KAKENHI Grant Number: JP26K15559) and the Inamori Foundation.

Existing connectome-based reservoir computing models have limitations in terms of the spatial scales of their model elements. While the edges connecting nodes in the reservoir layer are determined based on region-level, macroscopic connectome data, the node dynamics are modeled with artificial neural networks inspired by microscopic biological neural circuitry [2]–[8]. Thus, the spatial scales of the edges and node dynamics differ in the connectome-based reservoir, which compromises the interpretability of previous findings. Due to the difficulty of obtaining neuron-level, microscopic connectome data from the human brain, there is a demand for a connectome-based reservoir computing model that aligns the spatial scales of edges and node dynamics at the macroscopic level.

Thus far, spontaneous whole-brain activity has been simulated using a set of regional models of macroscopic neural dynamics, which are coupled based on the connectome [10]. Various mathematical models have been proposed to describe macroscopic neural dynamics [11], ranging from detailed conductance-based neural mass models [12]–[14] to simple oscillator models [15]–[17]. One such model that has been actively studied recently is the Stuart–Laudau oscillator model [18]–[20]. In this model, region-level oscillatory dynamics are described by the Stuart–Laudau equation, and each Stuart–Laudau oscillator is coupled with others according to structural connectivity weights with time delays derived from structural connectivity lengths. Cabral et al. [19] demonstrated that an intermediate global coupling constant for the oscillator ensemble yields metastability (i.e., fluctuations in the ensemble's synchrony level [21]), allowing for realistic simulations of macroscopic, spontaneous brain activity. However, there have been no reports of incorporating macroscopic neural dynamic models into connectome-based reservoir computing.

To address the issue of spatial scale mismatch, we develop a new connectome-based reservoir computing model, in which the node dynamics in the reservoir layer are determined by the macroscopic coupled Stuart–Laudau oscillators studied in [19]. We apply this model to a standard nonlinear transformation task to clarify its basic properties as a reservoir computing model. For this task, the connectome-based reservoir with coupled Stuart–Laudau oscillators is required to transform a sinusoidal input into a desired square output. We examine

how regression performance depends on the frequency and magnitude of the input. We also investigate the effects of the global coupling constant in the oscillator ensemble to clarify the relationship between performance and metastability—the key dynamic factor in reproducing macroscopic spontaneous brain activity. The data and code are available at https://github.com/makotofukushima/ijcnn2026.

II. Materials and Methods

A. Connectome Data

The connectome data used in this study is the same as the data adopted in [19], where the raw imaging data came from the WU-Minn Human Connectome Project [22]. We downloaded the matrices of undirected structural connectivity weights and lengths from https://github.com/fcast7/Hopf_Delay_Toolbox and used them to build the reservoir computing model detailed in the next section. Each node in these matrices is based on the automated anatomical labeling parcellation scheme [23] with $N = 90$ cortical and subcortical regions. More details about the connectome data can be found in [19].

B. Connectome-Based Reservoir Computing Model With Coupled Stuart–Landau Oscillators

Fig. 1 summarizes the structure of our new connectome-based reservoir computing model. The reservoir consists of a set of Stuart–Laudau oscillators coupled based on the connectome, which have been used for simulating macroscopic spontaneous brain activity [19]. Eq. (1) describes the oscillator dynamics of region (node) $n \in 1, \ldots, N$ as follows:

$$\begin{aligned}\frac{dz_n(t)}{dt} = {} & z_n(t)\{a + i\omega - |z_n(t)^2|\} \\ & + K\sum_{p\neq n}^{N} C_{n,p}\{z_p(t-\tau_{n,p}) - z_n(t)\} \\ & + \beta\{\eta_1(t) + i\eta_2(t)\} \\ & + (\mathbf{w}_{\mathrm{in}})_n k_{\mathrm{in}} x(t), \end{aligned} \tag{1}$$

where the complex variable $z_n(t)$ represents the state of oscillator n as a function of time t. The first line of Eq. (1) corresponds to the Stuart–Laudau equation for regional oscillation. Each oscillator had an angle frequency of $\omega = 2\pi \cdot 40$ Hz, which was used to model regional gamma-band neural oscillation [19]. The parameter a was set to -5 to generate realistic dumped oscillation dynamics [19].

The second line of the right-hand side of Eq. (1) represents the interaction term among structurally connected regions (oscillators). The n-th oscillator was influenced by the other oscillators through connectivity weights $C_{n,p}$ from the connectome data and time delays $\tau_{n,p}$. The connectivity weights were normalized so that the sum of all entries except the diagonal was 1, and the global coupling constant K set the strength of all regional interactions. The time delays $\tau_{n,p}$ were obtained by dividing connectivity lengths $L_{n,p}$ from the connectome data by the common conduction velocity v. We used representative parameter sets from [19], where K was 0.1, 10, or 50, and v was the velocity that yielded an average time delay of 5 ms.

The third line represents the noise term in the dynamic model. Variables $\eta_1(t)$ and $\eta_2(t)$ were white noise generated from the standard normal distribution. The scalar constant β for the noise was set to 0.001, as in [19].

The fourth line is the external input term to the reservoir, which is a new term added to the spontaneous brain activity model in [19]. The input time series $x(t)$ was scaled by its magnitude parameter k_{in}, as well as by the n-th entry of the N-dimensional input weights $\mathbf{w}_{\mathrm{in}}$. The input magnitude k_{in} was set to one of three values: 0.01, 0.1, or 1. The input weights $\mathbf{w}_{\mathrm{in}}$ were nonzero only at entries corresponding to regions that received the external input. In each simulation trial, 10 regions were randomly selected as input regions. Nonzero weights in $\mathbf{w}_{\mathrm{in}}$ were generated from a uniform distribution $U(-1, 1)$.

Eq. (1) was solved numerically using the Euler–Maruyama scheme with an integration step of $\Delta = 10^{-4}$ s [19]. Oscillator time series were generated for 55 s, after which the first 5 s were discarded.

When applied to the nonlinear transformation task, which is detailed in the next section, the readout regions were specified as all regions except the 10 input regions. The output time series $y(t)$ was computed from the real part of the states of the 80 readout oscillators $\mathrm{Re}(\mathbf{z}_{\mathrm{out}}(t))$ as follows:

$$y(t) = \mathbf{w}_{\mathrm{out}}^{\mathrm{T}} \mathrm{Re}(\mathbf{z}_{\mathrm{out}}(t)). \tag{2}$$

The output weights $\mathbf{w}_{\mathrm{out}}$ were learned to predict the desired output time series using ridge regression with a regularization constant of 10^{-10} [2]. The first and second halves of the time series were used as the training and test data, respectively.

C. Nonlinear Transformation Task

We applied the reservoir computing model described above to a nonlinear transformation task [24]–[27]. For this task, the reservoir had to transform a sinusoidal input $x(t)$ into a desired square output of 1 when $x(t) \geq 0$ and -1 otherwise (see Fig. 1). The frequency of the sinusoidal input varied from 0.5 Hz to 50 Hz in increments of 0.5 Hz.

Regression performance in this task was quantified using the coefficient of determination (R^2) and the normalized root mean square error (NRMSE), which was the RMSE normalized with the standard deviation of the desired output. We repeated the simulation and performance evaluation 100 times for each set of global coupling constant K, input magnitude k_{in}, and input frequency.

D. Characterization of the Dynamics of Oscillators

We characterized the dynamics of the ensemble of coupled oscillators using the order parameter:

$$R(t) = \left| \frac{1}{N} \sum_{n=1}^{N} e^{i\theta_n(t)} \right|, \tag{3}$$

where $\theta_n(t)$ is the phase of oscillator n. This phase was obtained by band-pass filtering $z_n(t)$ between $\max(0.1, f_{\mathrm{peak}} - 1)$ Hz and $f_{\mathrm{peak}} + 1$ Hz, where f_{peak} is the peak frequency of the ensemble, and then computing the instantaneous angle of

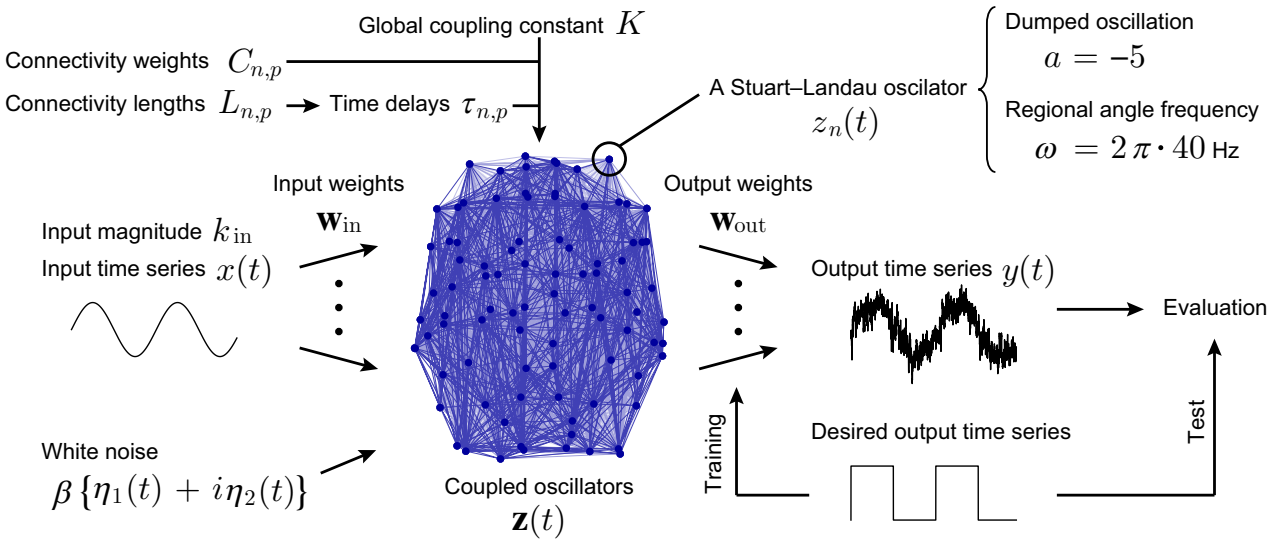

Fig. 1. An overview of the connectome-based reservoir computing model with coupled Stuart–Landau oscillators applied to a nonlinear transformation task. The brain graph of the connectome, viewed from above, is depicted as the reservoir in the center of the figure.

the filtered time series [19]. The peak frequency was calculated with a frequency resolution of 0.5 Hz.

The order parameter $R(t)$ measures the uniformity of oscillator phases and varies between 0 (fully desynchronized) and 1 (fully synchronized). The average synchrony level (global synchrony) and the fluctuations in synchrony (metastability) of the oscillator ensemble were quantified using the mean and standard deviation of $R(t)$, respectively [21].

III. Results

A. The Dynamics of Oscillators

Fig. 2 shows the peak frequency, global synchrony, and metastability of the ensemble of coupled oscillators in all simulation trials. When the input magnitude was relatively small ($k_{\text{in}} = 0.01$), the peak frequency was independent of the input frequency (Fig. 2A, left). Its median across all trials and input frequencies (39.5, 8.5, and 2.5 Hz for $K = 0.1$, 10, and 50, respectively) was identical to the median with no external input over 100 trials. As the input magnitude increased to $k_{\text{in}} = 0.1$, the peak frequency of a part of simulation trials equaled the input frequency (Fig. 2A, center). This proportion was 0.23, 0.64, and 0.11 for $K = 0.1$, 10, and 50, respectively, and increased to 0.83, 0.99, and 0.83 for $k_{\text{in}} = 1$ (Fig. 2A, right). The variation in proportion across the three K values indicates that intermediate global coupling ($K = 10$) enhances sensitivity to input.

Similar to the peak frequency, the global synchrony and metastability with a small input magnitude of $k_{\text{in}} = 0.01$ (Fig. 2B and C, left) were close to those observed with no external input (mean global synchrony of 0.13, 0.59, and 0.92, and mean metastability of 0.07, 0.18, and 0.09 when $K = 0.1$, 10, and 50, respectively). The metastable dynamics with intermediate global coupling ($K = 10$) [19] were reproducible, as shown here. Global synchrony and metastability with $k_{\text{in}} = 0.1$ and 1 exhibited characteristic profiles for simulation trials in which the peak frequency equaled the input frequency. In these trials, global synchrony was relatively higher when the input frequency was close to the peak frequency in the absence of external input (39.5, 8.5, and 2.5 Hz for $K = 0.1$, 10, and 50, respectively) (see Fig. 2B, center and right). These results suggest that the average synchrony level of the ensemble of coupled oscillators was increased by an input frequency similar to the "intrinsic" frequency of the oscillator ensemble with no external input. Fig. 2C (center and right) shows simulation trials with near-zero metastability (black regions in the heatmaps). These simulation trials were more evident with a larger input magnitude, $k_{\text{in}} = 1$.

B. Task Performance

Fig. 3 shows heatmaps and line plots of the performance metrics R^2 (Fig. 3A) and NRMSE (Fig. 3B) for the nonlinear transformation task. When $k_{\text{in}} = 0.01$ and the oscillator dynamics did not depend on the input frequency, the reservoir was unable to solve the task. With this small input magnitude, R^2 and NRMSE approached 0 and 1, respectively, in all simulation trials except for a few exceptional ones (Fig. 3A and B, left). Performance improved with larger input magnitudes. With $k_{\text{in}} = 0.1$, R^2 peaked and NRMSE valleyed around the input frequencies of 39.5, 8.5, and 2.5 Hz for $K = 0.1$, 10, and 50 (Fig. 3A and B, center). This suggests that the task is solved more easily when the input magnitude is closer to the intrinsic frequency of the oscillator ensemble. With a further large k_{in} value of 1, the peak of R^2 and the valley of NRMSE spread out horizontally (Fig. 3A and B, right).

Performance robustness against changes in input frequency varied with different values of the global coupling constant K when k_{in} was 0.1 and 1. The intermediate $K = 10$, which generates metastable dynamics if no external input is given, yielded the best performance at each input frequency over the largest proportion of input frequencies between 0.5 and 50 Hz

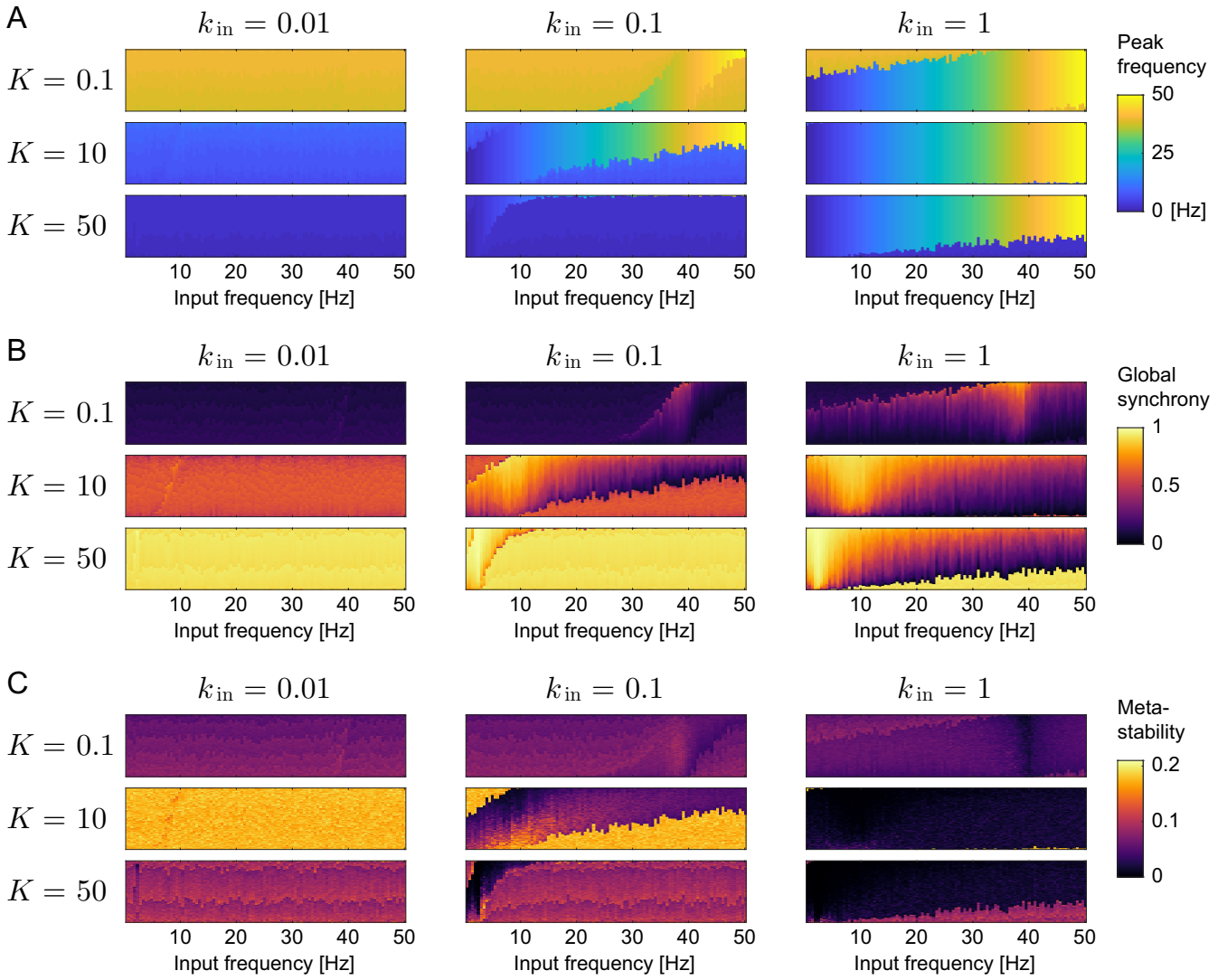

Fig. 2. The dynamics of the ensemble of coupled oscillators: (A) peak frequency, (B) global synchrony, and (C) metastability. Each dynamic metric is displayed in a heatmap for each simulation trial (vertical axis) and input frequency (horizontal axis). In each column of the heatmap in (A), the 100 simulation trials are sorted in descending order by peak frequency. The same trial orders are used in panels (B) and (C), where the simulation trials with the same peak frequency are sorted in descending order by global synchrony.

(see line plots in Fig. 3A and B, center and right). Conversely, simulation trials with higher performance partially overlapped with those exhibiting high global synchrony and near-zero metastability (see Fig. 3A and B, center and right, and Fig. 2B and C, center and right). These observations suggest that metastability during the task does not help solve the nonlinear transformation task. However, to achieve better performance for a wider range of input frequencies, the oscillator ensemble needs to be moderately coupled so that metastable dynamics are generated in the absence of external input.

IV. Discussion

To address the spatial scale mismatch between the edges and node dynamics in existing connectome-based reservoir computing models, we developed a new model that aligns these spatial scales at the macroscopic level using coupled Stuart–Laudau oscillators. We evaluated the basic properties of this model by applying it to a standard nonlinear transformation task, converting a sinusoidal input to a desired square output. For this task, we assessed regression performance by varying the input magnitude and frequency as well as the global coupling constant for the oscillator ensemble. When the input magnitude was small and the dynamic behavior of the oscillator ensemble was essentially the same as it was with no external input, the model's performance was low regardless of the input frequency or the global coupling constant. As the input magnitude increased, the ensemble's peak frequency was more likely to approach the input frequency, resulting in improved regression performance. Performance peaked when the input frequency was close to the ensemble's intrinsic frequency with no external input at each global coupling constant value. Regarding the relationship between performance and

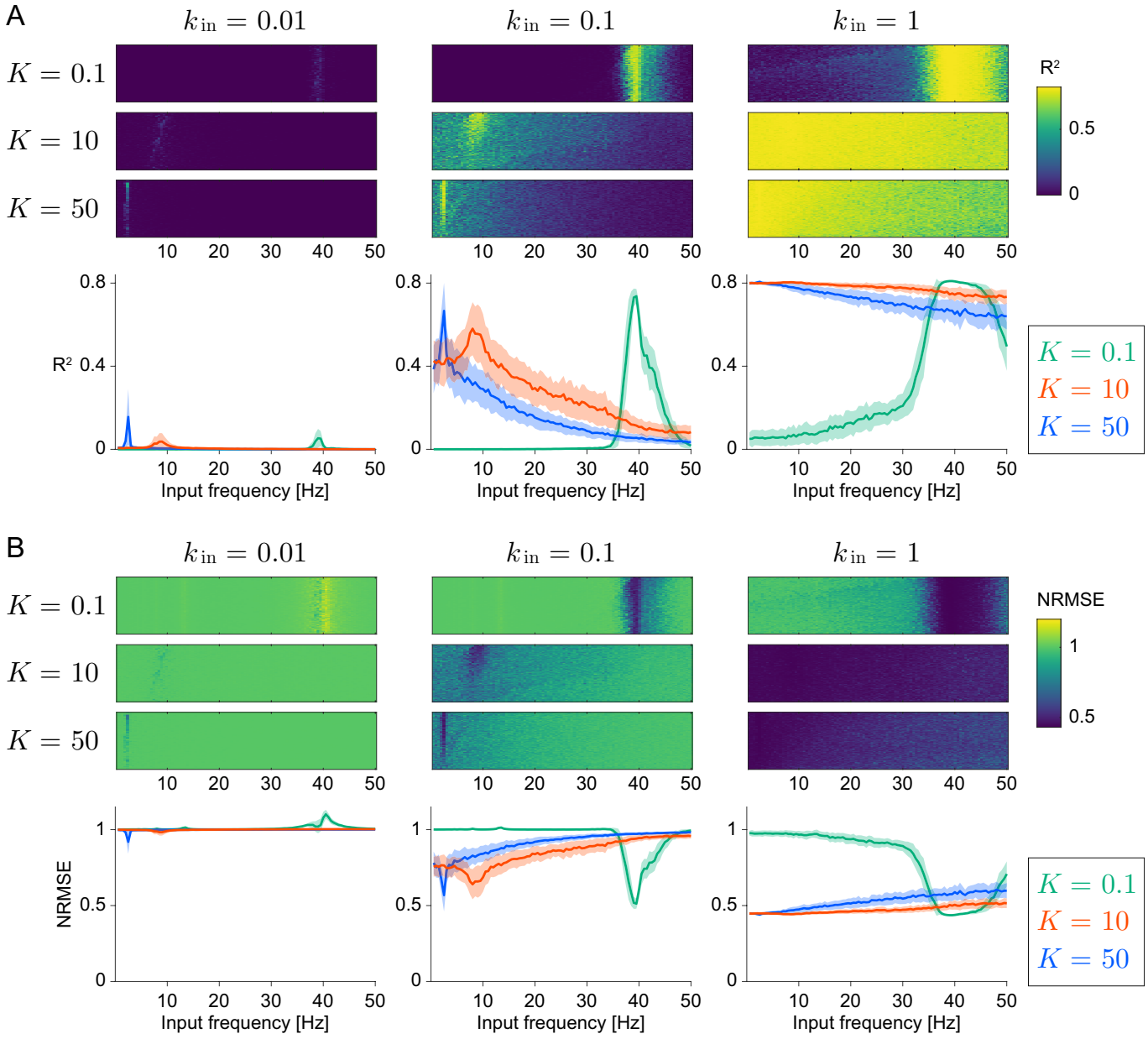

Fig. 3. Performance in the nonlinear transformation task: (A) coefficient of determination (R^2) and (B) normalized root mean square error (NRMSE). The orders of the simulation trials in the heatmaps in panels (A) and (B) are the same as in the heatmaps in Fig. 2A–C. Each line plot of the performance measures shows the mean and ± 1 standard deviation.

metastability, regression performance was not improved by metastability during the task; however, the oscillator ensemble with an intermediate level of global coupling that was capable of metastability with no external input exhibited the greatest robustness in performance against changes in input frequency.

Metastability is a key dynamic factor in simulating macroscopic, spontaneous brain activity [19]. Our analysis demonstrates that higher regression performance was achieved in the nonlinear transformation task when the oscillator ensemble was globally synchronized and had low metastability. This finding suggests that metastable dynamics during the task degrade performance in this task. However, the ability to exhibit noise-driven metastable dynamics without external input contributed to more robust regression performance in the face of fluctuations in input frequency. We speculate that this occurred due to the increased sensitivity to input exhibited by intrinsically metastable oscillators with $K = 10$ in Fig. 2A. In summary, the metastability of the oscillator ensemble in the absence of external input (i.e., not during the task) was useful for solving the nonlinear transformation task.

Although improving task performance was not our motivation for developing the new reservoir computing model, it should be noted that square wave regression was imperfect even at high input magnitudes and optimal input frequencies.

The best R^2 and NRMSE values in Fig. 3 were 0.81 and 0.44, respectively. This result was presumably obtained because the oscillatory dynamics of the new model face fundamental difficulties in regressing step functions. Additionally, the noise term in the equation of the node dynamics would be another factor degrading regression performance.

The performance assessment of the new connectome-based reservoir computing model has several limitations in this study. First, applying the model only to the nonlinear transformation task does not allow for evaluation of memory-related performance. The standard memory capacity task used in [2] and [3], for example, would be difficult for this model to solve because the dynamics of the oscillators are not suitable for regressing white noise time series. Memory capacity could be evaluated by modifying the nonlinear transformation task used in this study to shift the time samples of the desired output toward the past. Second, there is considerable room for improvement in terms of physiological realism. One way to address this issue would be to replace the current task with cognitive tasks that replicate those solved by the human brain. Setting the input and output regions in the reservoir to the visual and somatomotor regions in the connectome would also improve the model's physiological plausibility. A promising approach would be to incorporate the new model with coupled Stuart–Landau oscillators into the conn2res toolbox [6], so that we could apply it to cognitive tasks implemented by the NeuroGym software [28] using conn2res functions.

A potential next step in this study is to relate task performance to the model's ability to reproduce the empirical characteristics of actual neuroimaging data. Castaldo et al. [20] explored the two-dimensional parameter space of global coupling constants and mean time delays of coupled Stuart–Landau oscillators within cortical regions. They identified parameter sets that most accurately reproduced the empirical features of magnetoencephalography (MEG) data. We plan to apply the Stuart–Landau reservoir computing model with these parameter sets to various tasks and compare the results with those obtained using other parameter sets. This investigation could allow us to examine whether empirically plausible parameter sets achieve better performance in solving reservoir computing tasks.

REFERENCES

[1] O. Sporns, G. Tononi, and R. Kötter, "The human connectome: a structural description of the human brain," *PLOS Comput, Biol.*, vol. 1, no. 4, 2005, Art. no. e42.

[2] Y. Kawai, J. Park, and M. Asada, "A small-world topology enhances the echo state property and signal propagation in reservoir computing," *Neural Netw.*, vol. 112, pp. 15–23, 2019.

[3] L. E. Suárez, B. A. Richards, G. Lajoie, and B. Misic, "Learning function from structure in neuromorphic networks," *Nat. Mach. Intell.*, vol. 3, pp. 771–786, 2021.

[4] F. Damicelli, C. C. Hilgetag, and A. Goulas, "Brain connectivity meets reservoir computing," *PLOS Comput. Biol.*, vol. 18, no. 11, 2022, Art. no. e1010639.

[5] R. Nishimura and M. Fukushima, "Comparing connectivity-to-reservoir conversion methods for connectome-based reservoir computing," in *Proc. Int. Jt. Conf. Neural Netw. (IJCNN)*, 2024, doi: 10.1109/IJCNN 60899.2024.10650803.

[6] L. E. Suárez *et al.*, "Connectome-based reservoir computing with the conn2res toolbox," *Nat. Commun.*, vol. 15, 2024, Art. no. 656.

[7] A. Takahashi, L. Zhu, and M. Fukushima, "The role of brain connectivity patterns in applying connectome-based reservoir computing to neuroscience tasks," in *Proc. Int. Jt. Conf. Neural Netw. (IJCNN)*, 2025, doi: 10.1109/IJCNN64981.2025.11227896.

[8] M. Fukushima, "The effect of introducing randomness into connectome-based reservoir weights when solving neuroscience tasks," in *Proc. Int. Conf. Neural Inf. Process. (ICONIP)*, 2025, doi: 10.1007/978-981-95-4100-3_16.

[9] H. Jaeger, "The "echo state" approach to analysing and training recurrent neural networks," *GMD Report 148 (German National Research Center for Information Technology)*, 2001.

[10] M. Breakspear, "Dynamic models of large-scale brain activity," *Nat. Neurosci.*, vol. 20, no. 3, pp. 340–352, 2017.

[11] J. Cabral, M. L. Kringelbach, and G. Deco, "Functional connectivity dynamically evolves on multiple time-scales over a static structural connectome: models and mechanisms," *NeuroImage*, vol. 57, pp. 84–96, 2017.

[12] C. J. Honey, R. Kötter, M. Breakspear, and O. Sporns, "Network structure of cerebral cortex shapes functional connectivity on multiple time scales," *Proc. Natl. Acad. Sci. U. S. A.*, vol. 104, no. 24, pp. 10 240–10 245, 2007.

[13] C. J. Honey *et al.*, "Predicting human resting-state functional connectivity from structural connectivity," *Proc. Natl. Acad. Sci. U. S. A.*, vol. 106, no. 6, pp. 2035–2040, 2009.

[14] A. Zalesky, A. Fornito, L. Cocchi, L. L. Gollo, and M. Breakspear, "Time-resolved resting-state brain networks," *Proc. Natl. Acad. Sci. U. S. A.*, vol. 111, no. 28, pp. 10 341–10 346, 2014.

[15] J. Cabral, E. Hugues, O. Sporns, and G. Deco, "Role of local network oscillations in resting-state functional connectivity," *NeuroImage*, vol. 57, no. 1, pp. 130–139, 2011.

[16] M. Fukushima and O. Sporns, "Comparison of fluctuations in global network topology of modeled and empirical brain functional connectivity," *PLOS Comput, Biol.*, vol. 14, no. 9, 2018, Art. no. e1006497.

[17] M. Fukushima and O. Sporns, "Structural determinants of dynamic fluctuations between segregation and integration on the human connectome," *Commun. Biol.*, vol. 3, 2020, Art. no. 606.

[18] G. Deco, J. Cabral, M. W. Woolrich, A. B. A. Stevner, T. J. van Hartevelt, and M. L. Kringelbach, "Single or multiple frequency generators in on-going brain activity: a mechanistic whole-brain model of empirical MEG data," *NeuroImage*, vol. 152, pp. 538–550, 2017.

[19] J. Cabral *et al.*, "Metastable oscillatory modes emerge from synchronization in the brain spacetime connectome," *Commun. Phys.*, vol. 5, 2022, Art. no. 184.

[20] F. Castaldo *et al.*, "Multi-modal and multi-model interrogation of large-scale functional brain networks," *NeuroImage*, vol. 277, 2023, Art. no. 120236.

[21] M. Shanahan, "Metastable chimera states in community-structured oscillator networks," *Chaos*, vol. 20, no. 1, 2010, Art. no. 013108.

[22] D. C. Van Essen, S. M. Smith, D. M. Barch, T. E. J. Behrens, E. Yacoub, and K. Ugurbil for the WU-Minn HCP Consortium, "The WU-Minn Human Connectome Project: an overview," *NeuroImage*, vol. 80, pp. 62–79, 2013.

[23] N. Tzourio-Mazoyer *et al.*, "Automated anatomical labeling of activations in SPM using a macroscopic anatomical parcellation of the MNI MRI single-subject brain," *NeuroImage*, vol. 15, no. 1, pp. 273–289, 2002.

[24] H. O. Sillin *et al.*, "A theoretical and experimental study of neuromorphic atomic switch networks for reservoir computing," *Nanotechnology*, vol. 24, no. 38, 2013, Art. no. 384004.

[25] K. Fu *et al.*, "Reservoir computing with neuromemristive nanowire networks," in *Proc. Int. Jt. Conf. Neural Netw. (IJCNN)*, 2020, doi: 10.1109/IJCNN48605.2020.9207727.

[26] A. Loeffler *et al.*, "Modularity and multitasking in neuro-memristive reservoir networks," *Neuromorph. Comput. Eng.*, vol. 1, no. 1, 2021, Art. no. 014003.

[27] F. Milisav, A. I. Luppi, L. E. Suárez, G. Lajoie, and B. Misic, "Neuromorphic hierarchical modular reservoirs," *bioRxiv*, 2025, doi: 10.1101/2025.06.20.660760.

[28] M. Molano-Mazón *et al.*, "NeuroGym: an open resource for developing and sharing neuroscience tasks," *PsyArXiv*, 2022, doi: 10.31234/osf.io/aqc9n.